Zeeman ratchets: Rectification of spin current via magnetic fields

Matthias Scheid[1], Dario Bercioux[1,2], and Klaus Richter[1]

[1] Institut für Theoretische Physik, Universität Regensburg, D-93040 Regensburg, Germany

[2] Physikalisches Institut, Albert-Ludwigs-Universität, D-79104 Freiburg, Germany

E-mail: `Matthias.Scheid@physik.uni-regensburg.de`, `Dario.Bercioux@physik.uni-freiburg.de`

Abstract. We investigate the possibility of creating directed spin-polarized currents in a two-dimensional electron gas (2DEG) subject to an inhomogeneous magnetic field and an external adiabatic driving. We thereby generalize concepts of quantum charge ratchets to the case with spin. Due to the Zeeman term in the Hamiltonian, spin-up and -down electrons experience different effective potentials, which can be tailored to achieve net spin currents without corresponding charge currents. We consider ballistic, coherent transport in waveguides defined in a 2DEG, where the magnetic field modulation is induced by ferromagnetic stripes on top of the 2DEG.

Submitted to: *New J. Phys.*

1. Introduction

Spintronics as an emerging field of physics has attracted considerable attention in recent years and has developed into various inter-related branches covered in this topical issue. Spintronics is devoted to employ the spin degree of freedom for information storage and as another means for extending the functionality of electronic systems. Semiconductor spintronics, as one subfield, is guided by the idea of combining concepts of spin electronics with the established techniques and advantages of semiconductor physics and nanostructures. Up to now, their properties used mainly rely on the charge degree of freedom alone. Many ideas for employing spin-polarized currents have been put forward since the seminal propsal by Datta and Das for a spin transistor [1] based on spin precession controlled by an external electric field through spin-orbit coupling [2]. These proposals usually require spin injection, more generally, the creation of spin-polarized particles in these materials. Spin injection from a ferromagnetic metal source into semiconductors is hindered by a fundamental obstacle originating from the conductivity mismatch between these materials [3]. Though this problem may be partially circumvented, for instance at low temperatures by tailoring dilute-magnetic-semiconductor/semiconductor interfaces [4, 5] enabling considerable spin-polarization ratios of the order of 90% [4], all-semiconductor sources of spin-polarized electrons are still lacking.

Alternatively, several techniques to intrinsically create spin currents in non-magnetic systems have been put forward: Non-equilibrium spin-polarized currents have been created in two-dimensional electron gases (2DEGs) realized in zinc-blende-based heterostructures by means of optical pumping [6]. The irradiation of the 2DEG with circularly polarized light results in a spin photocurrent caused by the non-uniform distribution of the photoexcited carriers in **k**-space owing to optical selection rules and energy and momentum conservation. In the context of mesoscopic physics, further concepts such as adiabatic spin pumping [7, 8] and coherent spin ratchets [9, 10] have been proposed for generating spin-polarized currents. This can be achieved by exploiting the magnetic properties of the semiconducting material, i.e. intrinsic spin-orbit interaction or the Zeeman coupling to external magnetic fields.

Adiabatic quantum pumping involves the generation of a directed current in the absence of a bias voltage by periodic modulations of two or more system parameters, such as, *e.g.*, the shape of the system or a magnetic field [11]. The spin analog of the charge quantum pump can be achieved through an external magnetic field [7] or spin-orbit interaction [8] in order to filter the pumped current. For the case of an external magnetic field, it has been experimentally confirmed that under specific circumstances a spin current can be extracted from spin-dependent conductance fluctuations without accompanying net charge flow [12].

Ratchets [13] are generally systems with broken inversion (left/right) symmetry that generate directed net (particle) currents upon external AC driving in the absence of a net (time-averaged) bias potential. Thereby they have much in common with

current rectifiers, though there are differences, in particular in the dissipative case [13]. The theoretical concept of ratchets, originally introduced for classical dynamics, was extended to the quantum dissipative regime [14] and later experimentally realized in semiconductor heterostructures by demonstrating directed charge flow in a chain of asymmetric ballistic electron cavities in the low-temperature regime, where the dynamics was close to coherent [15].

Very recently, we have proposed the generalization of the ratchet mechanism, extensively explored for particle motion, to generate directed spin currents. Spin ratchets require a coupling to the electron spin which, e.g., can be provided via spin-orbit interaction or external (non-uniform) magnetic fields. In Ref. [9] *spin-orbit ratchets* have been considered in the coherent regime. There a proof of principle for a net ratchet spin current (in absence of an average charge current) has been given and confirmed by numerical calculations for experimentally accessible parameters for GaAs-based heterostructures.

In the present paper we further investigate the possibility of employing *Zeeman ratchets* for spin current generation, i.e. by considering mesoscopic conductors with a spatially varying Zeeman term and subject to an AC bias. In the simplest case of one-dimensional motion, and assuming preserved spin states, spin-up and -down electrons will experience a Zeeman term, $\pm(g^*/2)\mu_{\mathrm{B}}B(x)$, where $B(x)$ is the external non-uniform magnetic field, g^* the effective gyroscopic factor and μ_{B} the Bohr magneton. If $B(x) \neq B(-x)$, then the different spin species experience opposite asymmetric Zeeman ratchet potentials. In close analogy to the particle ratchet mechanism described above, the different spins are expected to be predominantly driven into opposite directions upon external driving, resulting in a spin-polarized current. This mechanism has been studied and confirmed in Ref. [10].

In the present work we relax both assumptions of one-dimensional motion [16] and conserved spin directions, *e.g.* the notion of two independent spin species, and explicitly include spin-flip effects. Moreover, we work out how such spin flip processes can be invoked to engineer and tune ratchet spin conductances. To this end we consider spin ratchet effects of a system consisting of a two-dimensional quantum wire embedded in 2DEG and subject to an AC bias in between two ohmic contacts. The non-uniform B-field is created by the magnetic fringe fields of ferromagnetic stripes patterned on the semiconductor heterostructure [17].

This paper is organized as follows: In Sec. 2 we introduce the model for the spin ratchet. We thereby specify the driving of the ratchet and the evaluation of the net charge and spin currents. In Sec. 3 we study transport through the quantum wire subject to the magnetic fringe fields of two ferromagnetic stripes with antiparallel magnetization perpendicular to the quantum wire in the plane of the 2DEG. This configuration (setup A in Fig. 1a) allows us to study the transition from decoupled to strongly coupled spin states and its implications on transport and thus also on the ratchet currents. In Sec. 4 we then investigate the conductor subject to the fringe field of a single ferromagnetic stripe magnetized perpendicular to the plane of the 2DEG (setup B in Fig. 1b)). Using
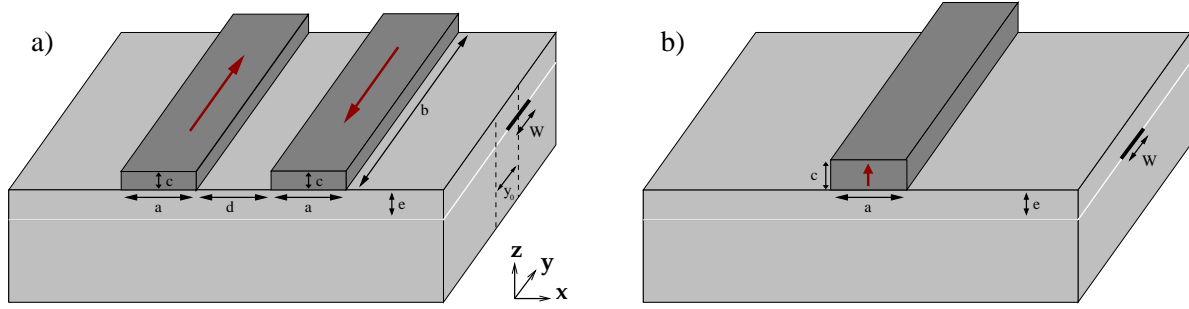
Figure 1. Ferromagnetic stripes (magnetization direction given by red arrows) on top of a semiconductor heterostructure that harbors a two-dimensional electron gas (indicated by white lines) containing a quantum wire (black) of width W. a) Setup A: two stripes with antiparallel in-plane magnetization, see Sec. 3; b) setup B: one stripe with out-of-plane magnetization, see Sec. 4.

symmetry arguments and numerical calculations we demonstrate that the two setups introduced in Sec. 3 and 4 act as spin ratchets. After summarizing in Sec. 5, we close the paper with an appendix on the general derivation of an expression for the spin current within the framework of the multi-terminal Landauer-Büttiker formalism and a second appendix including the derivation of symmetry relations for the transport properties at finite applied bias.

2. Model and formalism

We consider a quantum wire in the x-direction embedded in a 2DEG in the (x, y) plane. The system is subject to a non-uniform magnetic field $\vec{B}(x, y)$, due to the fringe fields of ferromagnetic stripes patterned on top of the 2DEG (see Fig. 1). Their deposition on a semiconductor heterostructure can be accomplished with electron beam lithography and lift-off techniques [18, 19]. Near-surface 2DEGs can be fabricated to lie only a few tens of nanometers beneath the surface [19], thereby achieving magnetic field values of up to 0.5T with thin ferromagnetic films [20]. The magnetic fringe field of a ferromagnet with homogeneous magnetization $\vec{M}$ is given by [21]

$$\vec{B}(\vec{r}) = -\frac{\mu_0}{4\pi} \vec{\nabla} \oint_S da' \, \frac{\vec{M} \cdot \hat{u}(\vec{r}')}{|\vec{r} - \vec{r}'|}, \tag{2.1}$$

where the integration runs over the surface S of the ferromagnetic stripe, and $\hat{u}(\vec{r}')$ is the unit vector normal to the surface of the stripe at position $\vec{r}'$. Accordingly, the corresponding vector potential in the Coulomb gauge, $\vec{\nabla} \cdot \vec{A} = 0$, is given by [21]

$$\vec{A}(\vec{r}) = \frac{\mu_0}{4\pi} \oint_S da' \frac{\vec{M} \times \hat{u}(\vec{r}')}{|\vec{r} - \vec{r}'|}. \tag{2.2}$$

We model the wire, where electron transport is assumed to be phase coherent, by the single-particle Hamiltonian

$$\hat{\mathcal{H}}_0 = \frac{\Pi_x(x, y)^2 + \Pi_y(x, y)^2}{2m^*} + \frac{g^* \mu_B}{2} \vec{B}(x, y) \cdot \vec{\sigma} + V(y), \tag{2.3}$$

where g^* is the effective gyroscopic factor, m^* the effective electron mass, μ_B the Bohr magneton and $\vec{\sigma}$ the vector of the Pauli matrices. The term $V(y)$ denotes the lateral confining potential defining the quantum wire. Orbital effects due to the magnetic field are accounted for by the vector potential $\vec{A}(x,y)$ in $\vec{\Pi}(x,y) = \vec{p} - e\vec{A}(x,y)$. Spin effects in transport through the wire enter via the Zeeman term $(g^*\mu_B/2)\vec{B} \cdot \vec{\sigma}$ coupling the spin degree of freedom to the external magnetic field. For a proper treatment of the spin evolution, the inclusion of the full magnetic field profile is mandatory [22]; disregarding [23] one of the magnetic field components B_i may lead to an oversimplification of the problem.

To obtain a significant spin ratchet effect materials with a large g^* factor are most suitable. In this respect dilute magnetic semiconductors (DMS) represent a promising class of materials. Recent measurements have shown values of $g^* > 100$ [24] where in addition to the intrinsic g-factor, an additional contribution to g^* appears, owing to exchange coupling among the electron spins and the magnetic ions present in the DMS [25].

In the present work where we consider disorder-free ballistic motion, we refer to nonmagnetic high-mobility semiconductors. To be definite we chose throughout the paper parameters for InAs 2DEGs with typical values of $m^* = 0.024 m_0$[26], where m_0 is the free electron mass, and $|g^*| = 15$. InAs is well suited due to its large g^* factor and the property that InAs 2DEGs can be fabricated close to the surface where the magnetic stripes are located. We assume that the stripes possess a magnetization $\mu_0 M = 3\text{T}$.

The charge current I_C through the wire is evaluated within the Landauer approach. For coherent transport in a two-terminal device the current can be expressed as

$$I_C = -\frac{e}{h} \int_0^\infty dE \left[f(E; \mu_L) - f(E; \mu_R)\right] T(E) \tag{2.4}$$

in terms of the quantum probability $T(E)$ for electrons with energy E to be transmitted from the lead at higher to the lead at lower potential. In Eq. (2.4), $f(E; \mu_{L/R})$ is the Fermi function for the left/right lead with chemical potential $\mu_{L/R}$.

The spin current $I_S(x)$ passing a cross section ($x = \text{const}$) is given, for a wavefunction $\Psi(x,y)$, by

$$I_S(x) = \int dy\, \Psi^*(x,y) \hat{J}_S \Psi(x,y)\,.$$

Here we use the most common definition [27] of the spin current operator $\hat{J}_S$ which, with respect to an arbitrary quantization axis $\hat{u}$, reads

$$\hat{J}_S = \frac{\hbar}{2} \frac{\hbar}{2m^*i} (\vec{\sigma} \cdot \hat{u}) \left(\frac{\overrightarrow{\partial}}{\partial x} - \frac{\overleftarrow{\partial}}{\partial x} \right) \tag{2.5}$$

inside the leads. The partial derivatives in (2.5) act on expressions to their right and left (indicated by the arrows).

Contrary to the charge current that obeys a continuity equation, the spin current can take different values if evaluated in the left or in the right lead. This usually happens in systems where the Hamiltonian does not commute with the Pauli matrices $\vec{\sigma}$ giving

rise to a torque inside the scattering region [28], which can change the spin state of the electrons. For this reason we will explicitly label the lead, where we compute the spin current. As derived in Appendix A (Eq. A.9) the corresponding spin current in the right lead reads

$$I_{\mathrm{S}} = \frac{1}{4\pi} \int_0^\infty \mathrm{d}E \, [f(E; \mu_{\mathrm{L}}) - f(E; \mu_{\mathrm{R}})] T_{\mathrm{S}}(E) \,, \tag{2.6}$$

with the spin transmission probability defined as

$$T_{\mathrm{S}}(E) = \sum_{\sigma=\pm 1} [T_{+,\sigma}(E) - T_{-,\sigma}(E)] \,. \tag{2.7}$$

Here $T_{\sigma',\sigma}$ is the probability for an electron with initial spin state σ to be transmitted from the left lead into the spin state σ' inside the right lead, see Eq. (A.7) in Appendix A. To obtain the corresponding spin current in the left lead one has to replace $T_{\sigma',\sigma}(E)$ in Eq. (2.7) by the corresponding probabilities $T'_{\sigma',\sigma}(E)$ for transmission from the right to the left lead.

Ordinary particle ratchets give rise to a net drift motion of particles in one preferential direction upon AC driving without net bias (rocking ratchet). Below we will generalize this concept to induce spin-dependent ratchet currents correspondingly. The AC driving can be considered as adiabatic, since the timescales for the variation of an external bias potential are long compared to the relevant time scales for charge transmission through the device. For a proof of principle we assume an adiabatic unbiased square-wave driving with period t_0. The system is periodically switched between two rocking conditions, labeled by bias $\pm U_0$ ($U_0 > 0$). The electro-chemical potential $\mu_{\mathrm{L/R}}$ of the left/right reservoir is changed periodically in time according to

$$\mu_{\mathrm{L/R}}(t) = \begin{cases} \varepsilon_{\mathrm{F}} \pm U_0/2 & \text{for} \quad 0 \le t < t_0/2 \\ \varepsilon_{\mathrm{F}} \mp U_0/2 & \text{for} \quad t_0/2 \le t < t_0 \end{cases}, \tag{2.8}$$

i.e. $\mu_{\mathrm{L/R}}(t) = \mu_{\mathrm{L/R}}(t + t_0)$. In the adiabatic limit considered, the system is assumed to be in a steady state between the switching events. Then the ratchet charge and spin currents inside the wire are obtained upon averaging Eqs. (2.4, 2.6) between the two rocking situations

$$\langle I_{\mathrm{C}}(\varepsilon_{\mathrm{F}}, U_0) \rangle = \frac{1}{2} \left[I_{\mathrm{C}}(\varepsilon_{\mathrm{F}}, +U_0) + I_{\mathrm{C}}(\varepsilon_{\mathrm{F}}, -U_0) \right] \tag{2.9a}$$

$$= -\frac{e}{2h} \int_0^\infty \mathrm{d}E \, \Delta f(E; \varepsilon_{\mathrm{F}}, U_0) \Delta T(E; U_0) \,,$$

$$\langle I_{\mathrm{S}}(\varepsilon_{\mathrm{F}}, U_0) \rangle = \frac{1}{2} \left[I_{\mathrm{S}}(\varepsilon_{\mathrm{F}}, +U_0) + I_{\mathrm{S}}(\varepsilon_{\mathrm{F}}, -U_0) \right] \tag{2.9b}$$

$$= \frac{1}{8\pi} \int_0^\infty \mathrm{d}E \, \Delta f(E; \varepsilon_{\mathrm{F}}, U_0) \Delta T_{\mathrm{S}}(E; U_0) \,,$$

where

$$\begin{aligned} \Delta f(E; \varepsilon_{\mathrm{F}}, U_0) &= f(E; \varepsilon_{\mathrm{F}} + U_0/2) - f(E; \varepsilon_{\mathrm{F}} - U_0/2), \\ \Delta T(E; U_0) &= T(E; +U_0) - T(E; -U_0), \\ \Delta T_{\mathrm{S}}(E; U_0) &= T_{\mathrm{S}}(E; +U_0) - T_{\mathrm{S}}(E; -U_0). \end{aligned} \tag{2.10}$$

An extension to an adiabatic harmonic driving is straight forward.

In linear response, the ratchet spin current $\langle I_S \rangle$, Eq. (2.9b), vanishes because $\Delta T_S(E; U_0 = 0) = 0$, see Eq. (2.10). Hence we must consider the nonlinear regime to obtain a finite net spin current. To model a finite voltage drop across the two leads, we add the term

$$\hat{\mathcal{H}}_U = U g(x, y; U) \tag{2.11}$$

to the Hamiltonian (2.3), where for the square wave driving considered here, U takes the values $\pm U_0$ respectively. Here the function $g(x, y; U)$ describes the spatial distribution of the electrostatic potential inside the mesoscopic system and is generally obtained through a self-consistent solution of the many-particle Schrödinger equation and the Poisson equation. However, here we employ heuristic models for $g(x, y; U)$, assuming that the voltage primarily drops in regions, where the magnetic field strongly varies spatially. This model is based on the fact that the corresponding Zeeman term acts as an effective potential barrier, and takes into account that a more rapid potential variation leads to enhanced wave reflection and hence to a steeper local voltage drop [29] (details will be given in the following sections).

In order to numerically evaluate the transport properties of the system, the stationary Schrödinger equation $(\hat{\mathcal{H}} - E)\Phi(\vec{r}) = 0$ is discretized on a square lattice, yielding a tight-binding representation of $\hat{\mathcal{H}}$. This is then used to calculate the elements of the scattering matrix of the system via lattice Greens functions and a recursive Greens function algorithm [30].

3. Setup A: Two ferromagnetic stripes with longitudinal magnitization

In this section we investigate the spin-dependent transport properties (and thereby also the operability as a ratchet) of a quantum wire in the plane of the 2DEG subject to the magnetic field of two stripes with opposite, longitudinal in-plane magnetizations, $\vec{M} = \pm M \hat{y}$, arranged perpendicular to the wire. This setup A is shown in Fig. 1a). The Hamiltonian of the system is given by Eq. (2.3) with $A_y = 0$ (in the Coulomb gauge), *i.e.* $\Pi_y = p_y$. For the following analysis we chose a confinement potential $V(y)$ such that the wire of width W is displaced by a shift y_0 with respect to the symmetric configuration, see Fig. 1.

For sufficiently narrow wires ($W \ll b$) and small displacement ($y_0 \ll b$), the energy scales of the magnetic field contributions to $\hat{\mathcal{H}}_0$ in Eq. (2.3) containing $\vec{B}$ and $\vec{A}$ are much smaller than differences between energy levels $E_m - E_n$ of different transversal modes $|m\rangle$ and $|n\rangle$. Therefore transitions between different transversal modes are strongly suppressed, and we consider the case of only one open mode. Higher modes $|n\rangle$ mimic the behavior of the first mode up to an energy offset $E_n - E_1$.

Evaluating Eq. (2.1) for the combined magnetic field of two stripes centered around $(x = 0, y = 0)$, setup A, we obtain the following symmetry properties for the B-field

components of this configuration:

$$B_x(x, -y, z) = -B_x(x, y, z), \tag{3.1a}$$

$$B_y(x, -y, z) = B_y(x, y, z), \tag{3.1b}$$

$$B_z(x, -y, z) = -B_z(x, y, z). \tag{3.1c}$$

In particular, Eqs. (3.1a) and (3.1c) imply vanishing magnetic field components B_x and B_z for $y = 0$. Therefore, we use $\hat{y}$ as the spin quantization axis for the considerations below. Those symmetries also have an important implication for the spin dynamics of the system. For a confinement potential that is symmetric upon reflection at the (x, z)-plane, $V(-y) = V(y)$, as realized for a symmetric confinement centered around $y_0 = 0$, spin-up and spin-down eigenstates within the same transversal mode n are decoupled. The relevant matrix element $\langle n, \sigma | \, \vec{\sigma} \cdot \vec{B}(x, y) \, | n, -\sigma \rangle$, responsible for the spin mixing, vanishes,

$$\int_{-\infty}^{\infty} dy |\chi_n(y)|^2 \Big[B_z(x, y) - i\sigma B_x(x, y) \Big] = 0, \tag{3.2}$$

since the integrand is an odd function of y due to Eqs. (3.1a,3.1c) and the fact that transversal modes obey $\chi_n(-y) = (-1)^{n-1}\chi_n(y)$. However, for finite values of y_0, the coupling (3.2) does not vanish anymore, and spin flips can arise with a significant effect on electron transport, as we will demonstrate in the next paragraph.

3.1. DC transport

Before evaluating the average charge current (2.9a) and spin ratchet current (2.9b) it is instructive to analyze the DC transport properties of setup A. To this end we chose as realistic parameters for the geometry (see Fig. 1(a)) $W = 120$ nm, $a = 600$ nm, $b = 2\mu$m (thus $W/b = 0.06$), $c = 200$ nm, $d = 600$ nm and $e = 100$ nm. For this parameter set and $y_0 \ll b$ the magnetic field component $B_y(x, y)$ is approximately constant in y-direction, i.e. $B_y(x, y) \approx B_y(x)$. It possesses a much larger maximum value than the other components B_x and B_z. In Fig. 2 we show the x-dependence of the overall magnetic fringe field of the two-stripe setup A for fixed $y = 200$nm.

Figure 3 shows the total transmission $T(E)$ in linear response ($U_0 \rightarrow 0$) for energies within the first transversal subband for different values of y_0. For $y_0 = 0$ the spin eigenstates decouple owing to Eq. (3.2). The energy where the first transversal mode opens is shifted to $E \approx E_1 + U_{\mathrm{B}}$ due to the Zeeman barrier of height $U_{\mathrm{B}} = g^* \mu_{\mathrm{B}} \max[B_y(x, y=0)]/2$ present in the wire. However, for increasing y_0 when spin flips can take place, an additional plateau builds up at energies $E_1 \leq E \leq E_1 + U_{\mathrm{B}}$ approaching $T \approx 1$. In the inset of Fig. 3 the spin-resolved transmission probabilities $T_{\sigma', \sigma}$ are depicted for $y_0 = 100$ nm. We identify $T_{+,-}(E)$ as the sole contribution to the total transmission $T(E)$ for $E_1 \leq E \leq E_1 + U_{\mathrm{B}}$. Thus the appearance of the additional plateau is a consequence of the mixing of the spin states. For energies well above the barrier both, spin-up and spin-down electrons are fully transmitted.
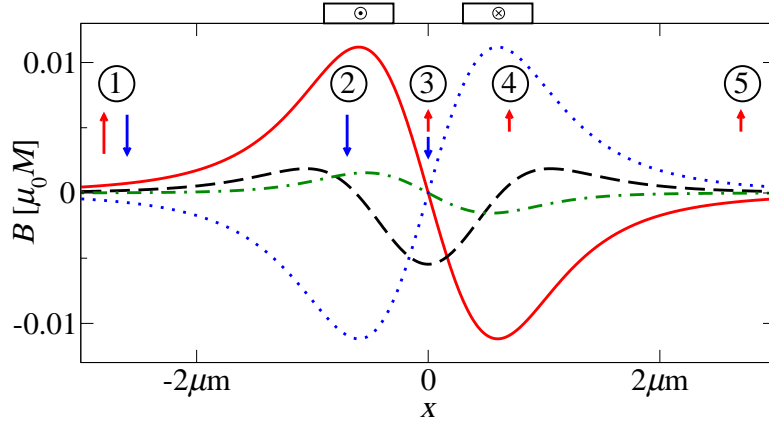
Figure 2. Magnetic field components B_x (dash-dotted green line), B_y (solid red), $-B_y$ (dotted blue) and B_z (dashed black) in the plane of the 2DEG at fixed $y = 200$nm for setup A, Fig. 1(a) and parameters given in the text.
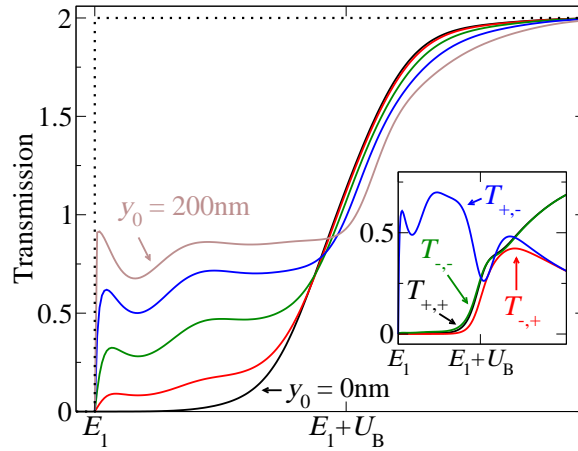
Figure 3. Total transmission $T(E)$ in linear response for values of $y_0 = 0$ nm to 200 nm in steps of 50 nm from bottom (black line) to top (brown line). The dotted black line indicates the transmission for $\vec{B} = 0$. Inset: spin-resolved transmission probabilities $T_{\sigma',\sigma}$, Eq. (A.7), for $y_0 = 100$ nm.

The main features in the numerically calculated transmission in Fig. 3 can be understood using a heuristic model. It is based on the fact that in the region close to $x = 0$ (see Fig. 2) spin flips predominantly take place, since $B_y(x,y) = 0$ vanishes at $x = 0$, and spin-up and -down states of the same transversal mode are nearly energy degenerate.

In the following we consider stepwise (positions labeled in Fig. 2) the spin evolution along the wire for unpolarized electrons entering the system with energy $E_1 \leq E \leq E_1 + U_B$:

(1) Unpolarized electrons (equal number of spin-up and spin-down particles) are injected from the left reservoir.

Zeeman ratchets: Rectification of spin current via magnetic fields

⓪ **2** Spin-up electrons are completely reflected at the Zeeman barrier (indicated by the solid red line), while spin-down electrons experience a potential valley (blue dotted line) and can pass.

3 A fraction of the spins is flipped from down to up due to a finite $B_z(x)$ close to $x = 0$.

4 Spin-down electrons are completely reflected while spin-up electrons pass.

5 Only spin-down electrons from the left lead reach the right lead, after undergoing a spin flip.

Hence this mechanism leads to $T_{+,+} = T_{-,+} = T_{-,-} = 0$ and $T_{+,-} \neq 0$. Although the model can explain the basic features of the transmission curves shown in Fig. 3 fairly well, it cannot account for the details in the functional dependence of $T(E)$ for energies below the barrier which reflects further quantum effects present, *e.g.* resonant tunneling processes. An analysis of the spin-resolved transmission probabilities in the opposite rocking situation, $\mu_{\rm L} < \mu_{\rm R}$, where electrons flow from right to left, shows that transmitted particles are oppositely spin-polarized compared with the former case. Correspondingly, $T'_{-,+}$ is the only non-zero component of the spin-resolved transmission for energies $E \leq E \leq E_1 + U_{\rm B}$.

The above analysis demonstrates that the magnetic field components perpendicular to the dominant one, even if they are small, can significantly alter the transport properties of the system. In the present case, disregarding B_x and B_z would have resulted in a vanishing transmission for $E < E_1 + U_{\rm B}$.

3.2. AC transport

We now investigate the rectification properties of setup A upon applying the AC driving given in Eq. (2.8). We first specify how we obtain the drop of the electrostatic potential $g(x, y; U)$ across the system for a finite applied bias. Based on a heuristic model used in Ref. [15] we assume that $(\partial g(x)/\partial x) \propto |(\partial/\partial x)B_y(x, y = 0)|$ in the central scattering region, $-L/2 < x < L/2$, yielding

$$g(x) = \frac{1}{2} - \frac{\int_{-L/2}^{x} {\rm d}x \, |(\partial/\partial x)B_y(x, y = 0)|}{\int_{-L/2}^{L/2} {\rm d}x \, |(\partial/\partial x)B_y(x, y = 0)|}, \tag{3.3}$$

while we fix $g(x)$ to $\pm 1/2$ inside the left (right) lead. For the full system Hamiltonian $\hat{\mathcal{H}} = \hat{\mathcal{H}}_0 + \hat{\mathcal{H}}_U$, Eqs. (2.3,2.11), at finite bias U_0 we evaluate the expressions (2.9a,2.9b) for the average charge and spin currents. If orbital effects due to the perpendicular magnetic field B_z are negligible, *i.e.* $A_y \simeq 0$, the total Hamiltonia $\hat{\mathcal{H}}$ is invariant under the symmetry operation $\hat{\mathcal{P}} = \hat{R}_x \hat{R}_U \sigma_z$. Then, as shown in Appendix B, the relation (B.4) between S-matrix elements holds true. Squaring S-matrix elements in Eq. (B.4) and summing over channels $(n\sigma) \in {\rm L}$ and $(n'\sigma') \in {\rm R}$ yields $T(E; \pm U_0) = T'(E; \mp U_0)$. This relation, together with the relation $T'(E; \mp U_0) = T(E; \mp U_0)$ due to unitarity of the S-matrix, leads to $\langle I_{\rm C} \rangle = 0$. A vanishing average charge current is in line with

symmetry considerations for charge ratchets and coincides with a numerical analysis for the parameters used here.

However, on the other hand, the symmetry considerations imply that the average spin current can take finite values. To confirm this numerically and to get an idea of its magnitude we calculate the ratchet spin current in the right lead according to Eq. (2.9b). Figure 4 shows the differences in spin transmissions, $\Delta T_S(E)$, for the two rocking situations as a function of energy for moderate finite applied bias voltage $U_0 = 0.1 U_B$. For $y_0 = 0$, where transitions between spin-up and spin-down states of the same transversal subband are absent, the system is comparable to the devices studied in Ref. [10]. There it was shown, in analogy to the case of charge rectification [31], that for conserved spin eigenstates the ratchet effect stems from different maximum values $\Delta_{\max}(U_0)$ of the effective potential landscape in the two rocking situations,

$$\Delta_{\max}(U_0) = \max[U_{\text{eff},\sigma}(x, +U_0)] - \max[U_{\text{eff},\sigma}(x, -U_0)], \tag{3.4}$$

with

$$U_{\text{eff},\sigma}(x, \pm U_0) = \pm U_0 g(x) + (\sigma/2)\mu_B g^* B_y(x, y = 0) \,. \tag{3.5}$$

This mechanism explains the rectification related to $\Delta T_{S;\hat{y}}(E; y_0 = 0)$ (solid black line in Fig. 4(b)) and its functional dependence for $y_0 = 0$. There spin flips are absent, and hence $T_{+,-} = T_{-,+} = 0$. For increasing y_0 the magnitude of $\Delta T_{S;\hat{y}}(E)$ decreases, while, at the same time, $\Delta T_{S;\hat{x}}(E)$ and $\Delta T_{S;\hat{z}}(E)$ grow and take finite values. Thus we can summarize that the ratchet effect survives in the presence of mixing of different spin states. However, as apparent from Fig. 4, the vector of spin polarization is no longer aligned along $\hat{y}$ for finite y_0.

We further study how sensitively the observed effect depends on the particular form of the voltage drop $g(x)$. To this end in Fig. 4 we additionally show ΔT_S for a linear voltage drop model $\tilde{g}(x) = -x/L$ (brown circles/triangles) inside the central region $(-L/2 < x < L/2)$, where the bias voltage $\tilde{U}_0$ was chosen such that the maximum value of the respective effective potential (3.5) was the same for both voltage drop models: $\max[U_{\text{eff},\sigma}(x, \pm U_0)] = \max[\tilde{U}_{\text{eff},\sigma}(x, \pm \tilde{U}_0)]$. Comparing $\Delta T_S(E; y_0)$ for $\tilde{g}(x)$ at $y_0 = 0$ (brown triangles) and 100 nm (brown circles) with the respective function $\Delta T_S(E; y_0)$ for $g(x)$ we observe no significant difference in their functional dependence on E, although the magnitude of the overall bias is different for both models ($\tilde{U}_0 \approx 2.3 U_0$ for the curves presented in Fig. 4). Therefore we can state that $\Delta T_S(E; y_0)$ rather depends on the difference (3.4) in the maximum values of the effective potential than the actual distribution of the electrostatic potential in the mesoscopic conductor. A study of ΔT_S in the other lead shows very similar results to the ones presented in Fig. 4.

In Fig. 5 we finally display the ratchet spin conductance $\langle I_S(\varepsilon_F, U_0)\rangle(e/U_0)$, Eq. (2.9$b$), which shows a nearly linear dependence on the bias voltage U_0, i.e. $\Delta T_S(E; y_0) \propto U_0$. This is in line with the above analysis showing that $\Delta T_S(E; y_0) \propto \Delta_{\max}(U_0)$ and $\Delta_{\max}(U_0) \propto U_0$.
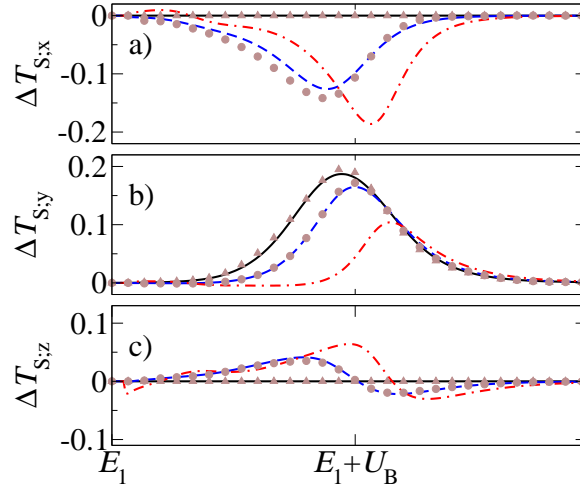
Figure 4. Ratchet spin transmission $\Delta T_{\rm S}$ for spin quantization axes $\hat{x}$ (Panel a), $\hat{y}$ (Panel b) and $\hat{z}$ (Panel c) as a function of the injection energy for displacement $y_0 = 0$ nm (solid black line), 100 nm (dashed blue) and 200 nm (dash-dotted red) for bias potential $U_0 = 0.1 U_{\rm B}$ and $g(x)$ specified in Eq. (3.3). For comparison, $\Delta T_{\rm S}$ at $y_0 = 0$ nm (brown triangles) and $y_0 = 100$ nm (brown circles) is shown for a linear voltage drop $\tilde{g}(x) = -x/L$ across the central scattering region with bias potential $\tilde{U}_0 \approx 2.3 U_0$.
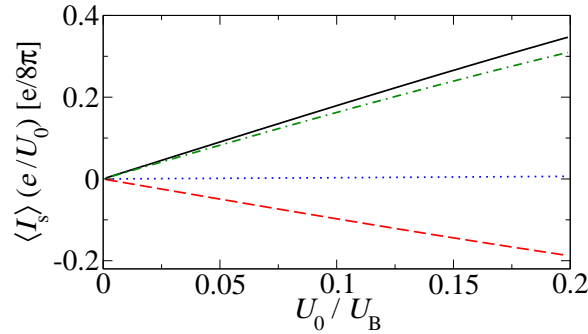

Figure 5. Bias voltage dependence of the ratchet spin conductance $\langle I_{{\rm S};\hat{u}} \rangle (e/U_0)$ at zero temperature, $k_{\rm B}T = 0$, for a Fermi energy $\varepsilon_{\rm F} = E_1 + U_B$. Results are shown for $y_0 = 0$ and polarization axis $\hat{u} = \hat{y}$ (black solid line), and for $y_0 = 100$ nm and $\hat{u} = \hat{x}$ (red dashed line), $\hat{y}$ (green dash-dotted line) and $\hat{z}$ (blue dotted line).

4. Setup B: a single ferromagnetic stripe with transverse magnetization

In the following we investigate the possibility of generating a spin ratchet effect using the magnetic field profile of a single stripe magnetized in the (x,z)-plane as shown in Fig. 1(b). For $b \gg W$ the evaluation of Eqs. (2.1,2.2) for a magnetization
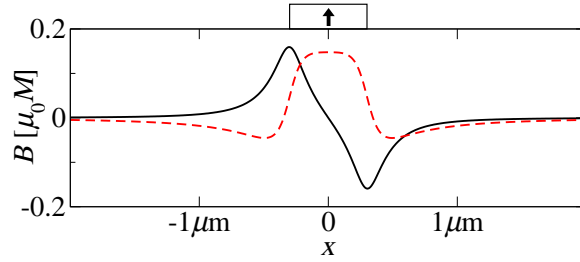
Figure 6. Magnetic field components $B_x(x)$ (solid black line) and $B_z(x)$ (dashed red line) in the plane of the 2DEG produced by a ferromagnetic stripe ($a = 600$ nm, $b \to \infty$, $c = 200$ nm, $e = 100$ nm, see Fig. 1(b)) with magnetization $\vec{M} = M\hat{z}$.
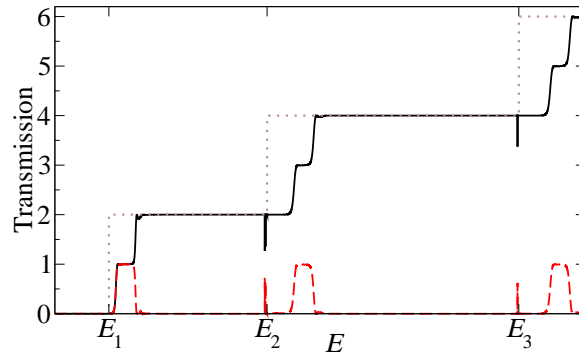
Figure 7. Total transmission $T(E)$ (solid black line) and absolute value of the spin transmission $|T_S|$ (dashed red line) as a function of energy for a wire underneath a single ferromagnetic stripe, see Fig. 1b and text. For comparison, the dotted brown staircase function shows the transmission in the absence of a magnetic field.

$\vec{M} = M_x\hat{x} + M_z\hat{z}$ yields

$$\vec{B}(\vec{r}) = \begin{pmatrix} B_x(x,z) \\ 0 \\ B_z(x,z) \end{pmatrix}, \quad \vec{A}(\vec{r}) = \begin{pmatrix} 0 \\ A_y(x,z) \\ 0 \end{pmatrix}.$$

The Hamiltonian of this system then reads

$$\hat{\mathcal{H}}_0 = \frac{p_x^2 + \Pi_y(x)^2}{2m^*} + g^* \frac{\mu_B}{2}\left[B_x(x)\sigma_x + B_z(x)\sigma_z \right] + V(y).$$

The 2DEG is located $e = 100$ nm below the surface of the semiconductor heterostructure (see Fig 1(b)). The extension of the stripe in x-direction is chosen to be $a = 600$ nm, infinite in y-direction and $c = 200$ nm in z-direction. For the analysis below we chose a stripe magnetization $\vec{M} = M\hat{z}$. The corresponding magnetic field in the plane of the 2DEG is depicted in Fig. 6. Results comparable to those presented below are obtained for a stripe magnetized in x-direction.

4.1. DC transport

In Fig. 7 we show the total transmission $T(E)$ for a quantum wire of width $W = 120\text{nm}$ subject to the B-field, Fig. 6, in linear response $(U_0 \to 0)$. In addition to the steps at even values of $T(E) \approx 2, 4, 6...$ due to the successive opening of the transversal modes at energies $E_n = [\hbar^2\pi^2/(2m^*W^2)]n^2$, additional plateaus appear at odd values of $T(E) \approx 1, 3, 5...$ close to the energies E_n. As in Section 3, we can attribute these features to the lifted spin degeneracy due to the Zeeman field, since also the width of these plateaus corresponds to twice the absolute height of the Zeeman barrier $U_\text{B} = (g^*/2)\mu_\text{B} \max[\,|\vec{B}|\,]$ inside the wire.

In Fig. 7 we furthermore plot the absolute value of the spin transmission, $|T_\text{S}| = \sqrt{(T_{\text{S};x})^2 + (T_{\text{S};y})^2 + (T_{\text{S};z})^2}$, which approaches unity at energies of the additional plateaus. A closer look at the spin- and mode-resolved transmission probabilities reveals that the transmission of the highest occupied transversal subband is completely spin polarized at the plateaus, while the lower modes are fully transmitting spin-up and spin-down particles. Similar results were reported in Ref. [22] for a stripe magnetized in the x-direction.

Apart from the spin effects due to the Zeeman term, the vector potential component A_y, affecting the orbital dynamics of the electrons due to the perpendicular magnetic field B_z, influences the electron transport. In a classical picture, B_z forces electrons to move on segments of cyclotron orbits in the plane of the 2DEG. Therefore, the kinetic energy in the direction of motion is reduced resulting in a shift of the energies where the transversal modes open towards higher values [32]. This is visible in Fig. 7, when comparing the total transmission with (solid black line) and without (dotted brown line) magnetic field.

4.2. AC transport

As for setup A we employ a heuristic model for the voltage drop inside the mesoscopic conductor, assuming $\partial g(x)/\partial x \propto |(\partial/\partial x)|\vec{B}(x)||$ inside the central region $(-L/2 < x < L/2)$ yielding

$$g(x) = \frac{1}{2} - \frac{\int_{-L/2}^{x} \text{d}x \left|(\partial/\partial x)|\vec{B}(x)|\right|}{\int_{-L/2}^{L/2} \text{d}x \left|(\partial/\partial x)|\vec{B}(x)|\right|}.$$

However, before we numerically investigate the AC ratchet transport properties, we exploit certain symmetries present in the system to simplify the expressions for the average net charge (2.9a) and spin currents (2.9b). For the magnetic field profile produced by a stripe magnetized in z-direction it is straightforward to show from Eqs. (2.1,2.2) that the following symmetry relations hold true (see also Fig. 6):

$$B_x(-x) = -B_x(x) \quad , \qquad B_z(-x) = B_z(x) \,,$$
$$A_y(-x) = -A_y(x) \quad , \qquad g(-x) = -g(x) \,.$$

Thus the Hamiltonian $\hat{\mathcal{H}} = \hat{\mathcal{H}}_0 + \hat{\mathcal{H}}_U$ is invariant under the action of the operator
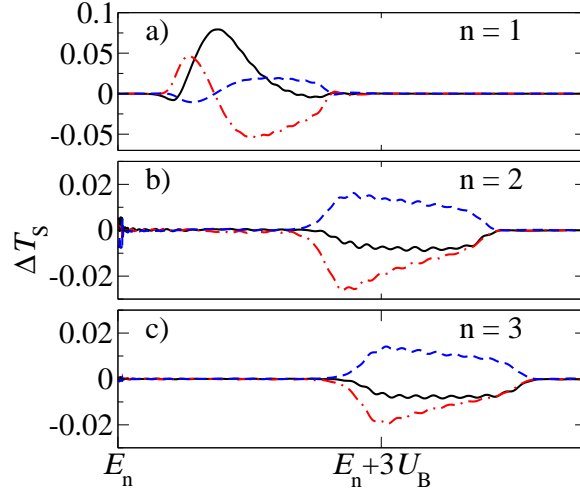
Figure 8. Averaged net spin transmission $\Delta T_{\mathrm{S}}(E; U_0)$ for spin polarization axis $\hat{x}$ (solid black line), $\hat{y}$ (dash-dotted red line) and $\hat{z}$ (dashed blue line) as a function of energy close to the lowest three transversal energy levels E_n $(n = 1, 2, 3)$ for an applied bias voltage of $U_0 = 0.1 U_{\mathrm{B}}$.

$\hat{\mathcal{P}} = -\mathrm{i}\hat{\mathcal{C}}\hat{R}_x\hat{R}_U\sigma_z$, where $\hat{\mathcal{C}}$ is the operator of complex conjugation, $\hat{R}_x$ inverses the x-coordinate, $\hat{R}_U$ changes the sign of the applied voltage $(\pm U_0 \leftrightarrow \mp U_0)$ and σ_z is the Pauli spin operator. Due to $[\hat{\mathcal{H}}, \hat{\mathcal{P}}] = 0$ we are able to interrelate the transmission probabilities for both rocking situations as shown in Appendix B. Taking the square of Eq. (B.3) and summing over the transversal modes $n \in \mathrm{L}$ and $n' \in \mathrm{R}$ we obtain the following relations between the spin-resolved transmission probabilities in the two rocking situations:

$$T_{\sigma,\sigma'}^{(\theta,\phi)}(E, \pm U_0) = T_{\sigma',\sigma}^{(\theta,-\phi+\pi)}(E, \mp U_0).$$

Here the superscript labels the angles of the spin quantization axis on the Bloch sphere (see Appendix B). Thus the ratchet charge current (2.9a) vanishes,

$$\langle I_{\mathrm{C}}(\varepsilon_{\mathrm{F}}, U_0)\rangle = 0,$$

and we can express the ratchet spin current (2.9b) through the transmission probabilities of a single rocking situation (*e.g.* $+U_0$):

$$\langle I_{\mathrm{S};x}(\varepsilon_{\mathrm{F}}, U_0)\rangle = \frac{1}{4\pi} \int_0^\infty \mathrm{d}E \, \Delta f(E; \varepsilon_{\mathrm{F}}, U_0) \times$$
$$\times \left[T_{+,+}(E, +U_0) - T_{-,-}(E, +U_0)\right],$$
$$\langle I_{\mathrm{S};y/z}(\varepsilon_{\mathrm{F}}, U_0)\rangle = \frac{1}{4\pi} \int_0^\infty \mathrm{d}E \, \Delta f(E; \varepsilon_{\mathrm{F}}, U_0) \times$$
$$\times \left[T_{+,-}(E, +U_0) - T_{-,+}(E, +U_0)\right].$$

Figure 8 shows the ratchet spin transmission $\Delta T_{\mathrm{S}}(E; U_0)$ at a finite applied voltage $U_0 = 0.1 U_B$ for a wire of width $W = 120$ nm. This quantity is finite for energies where the DC transmission is spin polarized (see Fig. 7). Furthermore, the spin polarization of the ratchet spin transmission depends on the injection energy. This opens the possibility
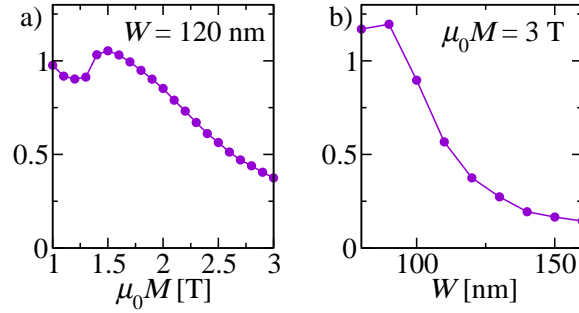
Figure 9. Ratio $\Delta T_{\mathrm{S,max}}(n = 2)/\Delta T_{\mathrm{S,max}}(n = 1)$ as a function of (a) the magnetization of the ferromagnetic stripe and (b) the wire width.
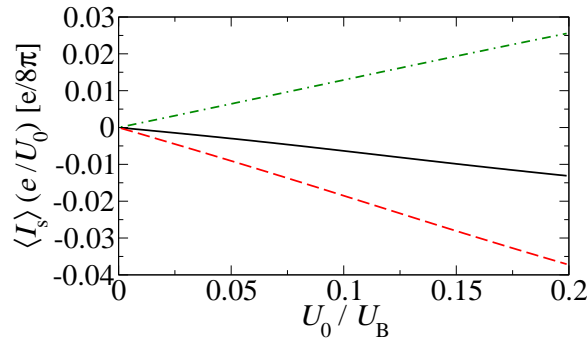
Figure 10. Ratchet spin conductance $\langle I_{\mathrm{S},\hat{u}}\rangle(e/U_0)$ as a function of bias voltage U_0 at $k_{\mathrm{B}}T = 0$ and $\varepsilon_{\mathrm{F}} = E_3 + 3U_B$ for the spin quantization directions $\hat{x}$ (black solid line), $\hat{y}$ (red dashed line) and $\hat{z}$ (green dash-dotted line).

to tune it upon varying the Fermi energy. Comparing the ratchet spin transmission for $n = 1$ (Panel a) and $n = 2, 3$ (Panels b,c) we observe that its magnitude is significantly lower in the case where more than one transversal mode is conducting. This behavior is due to the mixing of different transversal subbands due to $A_y(x)$. To quantify this effect we introduce

$$\Delta T_{\mathrm{S,max}}(n) = \max_{E \in [E_n, E_{n+1}]} \left[\sqrt{\Delta T_{\mathrm{S};\hat{x}}(E)^2 + \Delta T_{\mathrm{S};\hat{y}}(E)^2 + \Delta T_{\mathrm{S};\hat{z}}(E)^2} \right]$$

as a measure for the rectification in each single transversal mode. Figure 9 shows that $\Delta T_{\mathrm{S,max}}(n = 2)/\Delta T_{\mathrm{S,max}}(n = 1) \approx 1$ for cases where the mixing due to $A_y(x)$ is small, *i.e.* for a narrow wire and/or small magnetic field. However it decreases upon increasing $\mu_0 M$ and/or W. Note that for setup A in the previous section the magnetic field inside the quantum wire was one order of magnitude smaller than for setup B here, thus yielding a comparable value $\Delta T_{\mathrm{S,max}}(n)$ for all subbands n.

As for setup A, the ratchet spin conductance shown in Fig. 10 exhibits a linear dependence on the applied voltage. Thus we presume that the rectification mechanism is the same as in setup A, although the spin dynamics is much more intricate.

5. Conclusions and Outlook

In the present work we have shown that the coupling of the electron spin to the magnetic fringe fields of ferromagnetic stripes via the Zeeman interaction can be used to generate a spin ratchet effect in a coherent mesoscopic conductor subjected to an adiabatic AC driving with finite bias. The proposed devices exhibit the appealing property of creating a directed net spin current in the absence of an accompanying net charge transport. This key result has been demonstrated in numerical approaches for setups A and B, in the case of setup B, also analytically based on symmetry properties of the system.

The generated spin current may be regarded as resulting from a rectification effect, however in a generalized sense: The direct analogue of a charge current rectifier would be a system generating a directed spin current out of a conductor with alternating *spin-chemical* potentials in the left and right reservoir. Spin ratchets, as the ones considered here, act differently as they convert an AC *electrical* bias into a net spin current.

From our analysis we have identified the difference in the maximum values of the effective Zeeman potentials in the respective rocking situations as responsible for the creation of the spin current. It has been shown that this rectification effect is almost independent of the actual distribution of the electrostatic potential in the biased conductor. Furthermore, the fact that, for the systems considered here, the difference in the maximum values of the Zeeman potential is crucial for the spin currents, implies that the magnitude of the spin current cannot be systematically increased upon increasing the number of magnetic stripes, e.g. in a periodic arrangement of stripes. We have checked this also numerically by adding an increasing number of stripes.

In the preceding sections we presented results, when evaluating the spin current inside the right lead. However, as we noted both systems considered, setup A and B, are characterized by interesting symmetry properties. Those can now be used to directly extract the respective currents inside the left lead. If for setup A the component A_x can be neglected, as it is appropriate for the parameters used in Sec. 3, the combined Hamiltonian of the system and the leads has been proven to be invariant under the action of the symmetry operation $\hat{R}_x\hat{R}_y\hat{R}_U\sigma_z$, while for setup B the Hamiltonian is invariant under the action of $\hat{R}_x\hat{R}_U\sigma_z$. These symmetry properties are reflected in Eqs. (B.4) and (B.5) respectively, see Appendix B. Both relations lead to the general relation

$$T'^{(\theta,\phi+\pi)}_{\sigma,\sigma'}(E,\mp U_0) = T^{(\theta,\phi)}_{\sigma,\sigma'}(E,\pm U_0)$$

between the transmission probabilities in the two rocking situations. This relation allows for the following interpretation. If the transmitted electrons are spin-polarized in one of the two rocking situations with direction of the polarization vector given by the angles (θ,ϕ) on the Bloch sphere, then in the other rocking situation the spin polarization vector of the output current (in the other lead) will be rotated around the z-axis by π and thus points to $(\theta,\phi+\pi)$. This property is a direct consequence of the lacking conservation of the spin eigenstates inside the wire.

The physics of semiconducting materials characterized by a large g^* factor is dominated by the presence of magnetic impurities, *e.g.* diluted magnetic semiconductors [25].

Therefore, in order to exploit the expected stronger rectification effect, we have to take elastic scattering off impurities into account. In particular, we plan to study how additional disorder alters the spin ratchet effects.

Finally, since the heuristic model used for the distribution of the electrostatic potential in the conductor is convenient but not fully satisfactory, it would be desirable to calculate the charge density and the respective electrostatic potential inside the wire self-consistently. Work in this direction is in progress.

Acknowledgments

Appendix A. Calculation of the spin current in the Landauer-Büttiker formalism

In this appendix we present a derivation of the expressions for spin current in the leads of a multiterminal coherent conductor within the framework of the Landauer-Büttiker theory [33]. To this end we consider N non-ferromagnetic contacts, injecting spin-unpolarized current into the leads. For convenience we use a local coordinate system for the lead under investigation, where x is the coordinate along the lead in the direction of charge propagation due to an applied bias in linear response and y is the transverse coordinate. Then the eigenfunctions inside a lead are given by

$$\Phi^{\pm}_{E,n\sigma}(x,y) = \frac{1}{\sqrt{k_x(E)}} e^{\pm ik_x(E)x} \chi_n(y)\Sigma(\sigma) \tag{A.1}$$

where the $\chi_n(y)$ are the transverse eigenfunctions of the lead with the transversal eigenenergy E_n and $\Sigma(\sigma)$ is the spin eigenfunction. The superscript $\pm$ of Φ refers to the direction of motion in $\pm x$-direction with the wave-vector $k_x = \sqrt{2m^*(E-E_n)}/\hbar$. For the derivation we use the scattering approach, where the amplitudes of the states inside the leads are related via the scattering matrix $\mathbf{S}(E)$, determined by the Hamiltonian of the coherent conductor. Inside lead q a given scattering state

$$\varphi^q_E(x,y) = \sum_{(n\sigma)\in q} \left(a^q_{n\sigma}(E)\Phi^+_{E,n\sigma}(x,y) + b^q_{n\sigma}(E)\Phi^-_{E,n\sigma}(x,y) \right),$$

($\sigma = \pm$), consists of incoming states Φ^+ entering the coherent conductor from contact q and outgoing states Φ^- leaving the coherent conductor into contact q. The amplitudes of incoming $a^j_{n\sigma}$ and outgoing waves $b^i_{n'\sigma'}$ are related via the equation

$$b^i_{n'\sigma'}(E) = \sum_{j=1}^{N} \sum_{n\in j} \sum_{\sigma=\pm 1} S^{i,j}_{n'\sigma',n\sigma}(E) a^j_{n\sigma}(E), \tag{A.2}$$

where the scattering matrix $\mathbf{S}(E)$ has the following structure for an N terminal system:

$$
\mathbf{S}(E) = \begin{pmatrix} \mathbf{r}^{1,1}(E) & \mathbf{t}^{1,2}(E) & \cdots & \mathbf{t}^{1,N}(E) \\ \mathbf{t}^{2,1}(E) & \mathbf{r}^{2,2}(E) & \cdots & \mathbf{t}^{2,N}(E) \\ \vdots & \vdots & \ddots & \vdots \\ \mathbf{t}^{N,1}(E) & \mathbf{t}^{N,2}(E) & \cdots & \mathbf{r}^{N,N}(E) \end{pmatrix}.
$$

Here the sub-matrix $\mathbf{r}^{j,j}(E)$ is a square matrix of dimensionality $M^j(E)$, corresponding to the number of open channels at energy E in lead j (already including the spin degree of freedom), which is connected to a reservoir with chemical potential μ_j. The matrix $\mathbf{r}^{j,j}(E)$ contains the scattering amplitudes of incoming channels of lead j being reflected back into outgoing channels of the same lead. The sub-matrix $\mathbf{t}^{i,j}(E)$ is a $M^i(E) \times M^j(E)$ matrix that contains the scattering amplitudes for transmission between incoming channels from lead j and outgoing channels of lead i.

The wave function of the scattering state inside lead i, where only the incoming channel $(n\sigma) \in j$ is populated $(a_{n'\sigma'}^{j'} = \delta_{j',j}\delta_{n',n}\delta_{\sigma',\sigma})$, reads for $j = i$:

$$
\varphi_{E,n\sigma}^i(x,y) = \Phi_{E,n\sigma}^+(x,y) + \sum_{(n'\sigma')\in i} r_{n'\sigma',n\sigma}^{i,i}(E)\Phi_{E,n'\sigma'}^-(x,y), \tag{A.3}
$$

and, correspondingly, for $j \neq i$

$$
\varphi_{E,n\sigma}^i(x,y) = \sum_{(n'\sigma')\in i} t_{n'\sigma',n\sigma}^{i,j}(E)\Phi_{E,n'\sigma'}^-(x,y). \tag{A.4}
$$

For a wave function $\Psi(x,y)$ the spin current $I_{\mathrm{S}}^\Psi(x)$ passing a cross section $(x = \text{const})$ of a lead is given by:

$$
I_{\mathrm{S}}^\Psi(x) = \int \mathrm{d}y\, \Psi^*(x,y)\hat{J}_{\mathrm{S}}\Psi(x,y). \tag{A.5}
$$

Here we use the most common definition of the spin current operator [27], which with respect to an arbitrary quantization axis $\hat{u}$ takes the following form inside the leads:

$$
\hat{J}_{\mathrm{S}} = \frac{\hbar}{2}\frac{\hbar}{2m^*i}(\vec{\sigma}\cdot\hat{u})\left(\overrightarrow{\frac{\partial}{\partial x}} - \overleftarrow{\frac{\partial}{\partial x}}\right).
$$

The partial derivatives act on the expressions to their right/left respectively (indicated by the arrows). For the scattering state (A.3) we then obtain for the spin current (A.5) inside lead i

$$
I_{\mathrm{S};E,n\sigma}^{j=i}(x \in i) = \frac{\hbar^2}{2m^*}\left[\sigma - \sum_{(n'\sigma')\in i} \sigma' \left|r_{n'\sigma',n\sigma}^{i,i}(E)\right|^2\right],
$$

where $(n\sigma \in j, j = i)$. For the scattering state (A.4) we find the corresponding expression $(n\sigma \in j, j \neq i)$

$$
I_{\mathrm{S};E,n\sigma}^{j\neq i}(x \in i) = -\frac{\hbar^2}{2m^*}\sum_{(n'\sigma')\in i} \sigma' \left|t_{n'\sigma',n\sigma}^{i,j}(E)\right|^2.
$$

Since every channel is populated according to the Fermi-Dirac distribution $f(E;\mu_q)$ of the respective contact q, the total spin current in lead i then reads

$$I_{\mathrm{S}}(x \in i) = \frac{m^*}{2\pi\hbar^2} \int_0^\infty \mathrm{d}E \left[\sum_{j=1}^N \sum_{(n\sigma)\in j} f(E;\mu_j) I^j_{\mathrm{S};E,n\sigma}(x \in i) \right] \tag{A.6}$$

$$= \frac{-1}{4\pi} \int_0^\infty \mathrm{d}E \left[f(E;\mu_i) R_{\mathrm{S}}^{i,i}(E) + \sum_{q\neq i} f(E;\mu_q) T_{\mathrm{S}}^{i,q}(E) \right]$$

where

$$T_{\mathrm{S}}^{i,q}(E) = \sum_{\sigma'=\pm} \left(T_{+,\sigma'}^{i,q} - T_{-,\sigma'}^{i,q} \right)$$

$$R_{\mathrm{S}}^{i,i}(E) = \sum_{\sigma'=\pm} \left(R_{+,\sigma'}^{i,i} - R_{-,\sigma'}^{i,i} \right) ,$$

and

$$T_{\sigma,\sigma'}^{i,q}(E) = \sum_{n\in i} \sum_{n'\in q} \left| t_{n\sigma,n'\sigma'}^{i,q}(E) \right|^2 , \tag{A.7}$$

$$R_{\sigma,\sigma'}^{i,i}(E) = \sum_{n\in i} \sum_{n'\in i} \left| r_{n\sigma,n'\sigma'}^{i,i}(E) \right|^2 . \tag{A.8}$$

Since $\mathbf{S}(E)$ is unitary, the following relation holds true:

$$\sum_{(n'\sigma')\in i} \left| r_{n\sigma,n'\sigma'}^{i,i}(E) \right|^2 + \sum_{q\neq i} \sum_{(n''\sigma'')\in q} \left| t_{n\sigma,n''\sigma''}^{i,q}(E) \right|^2 = 1.$$

Then it is straightforward to show that

$$R_{\mathrm{S}}^{i,i}(E) + \sum_{q\neq i} T_{\mathrm{S}}^{i,q}(E) = 0,$$

In view of Eq. (A.6) we eventually find for the spin current in lead i

$$I_{\mathrm{S}}(x \in i) = \frac{1}{4\pi} \int_0^\infty \mathrm{d}E \sum_{q\neq i} \left[f(E;\mu_i) - f(E;\mu_q) \right] T_{\mathrm{S}}^{i,q}(E). \tag{A.9}$$

Equation (A.9) obviously shows that in thermal equilibrium ($\mu_j = \mu$) the spin current inside the leads vanishes. This absence of equilibrium spin currents in the leads has been shown for systems with preserved time-reversal symmetry [34]. However, here we show that it is more generally valid for any coherent conductor, since we did not make any assumptions about symmetries of the scattering region in the course of the derivation.

We note that the relation (5) derived in Ref. [35] that allows for equilibrium spin currents, has to be regarded as incorrect, arising from an improper treatment of the back-reflection, missing the term

$$\frac{1}{4\pi} \int_0^\infty \mathrm{d}E \, f(E;\mu_i) 2 \left(R_{-,+}^{i,i}(E) - R_{+,-}^{i,i}(E) \right) \tag{A.10}$$

in comparison with Eq. (A.9). This issue has been addressed by Nikolic *et al.* [36]. However, their argumentation that the term (A.10) has only to be included in equilibrium, *i.e.* for energies up to the lowest chemical potential of the N terminals,

seems questionable. If the spin current is evaluated in a lead connected to a reservoir k with $\mu_k > \mu_l$ (μ_l being the lowest chemical potential of any of the N reservoirs), the full expression (A.9) has to be used.

Our results are confirmed by recent publications on the mesoscopic spin Hall effect [38] using a simplified version of Eq. (A.9),

$$I_{\rm S} = \frac{1}{4\pi} \sum_{q \neq i} (\mu_i - \mu_q) T_{\rm S}^{i,q},$$

where transport at zero temperature and energy-independent transmission probabilities were considered.

Appendix B. Derivation of symmetry relations for spin dependent Landauer transport at finite bias

Here we derive symmetry relations for a two terminal setup as used in this Paper. We generalize related expressions from Ref. [39] to finite bias and arbitrary spin quantization axis.

If the Hamiltonian of the total system of scattering region and leads is invariant under certain symmetry operations $\hat{\mathcal{P}}$, we can relate the elements of the scattering matrix even in different rocking situations. As an example we derive the symmetry relations stemming from the symmetry operator $\hat{\mathcal{P}} = -\mathrm{i}\hat{\mathcal{C}}\hat{R}_x\hat{R}_U\sigma_z$, where $\hat{\mathcal{C}}$ is the operator of complex conjugation, $\hat{R}_x$ inverts the x-coordinate, $\hat{R}_U$ changes the sign of the applied voltage ($\pm U_0 \leftrightarrow \mp U_0$) and σ_z is the Pauli spin operator.

Generalizing Eq. (A.1) of Appendix A the eigenfunctions inside the leads are given by

$$\Phi_{E,n\sigma}^{\pm,(\theta,\phi)}(x,y) = \frac{1}{\sqrt{k_x(E)}} e^{\pm \mathrm{i}k_x(E)x} \chi_n(y) \Sigma_{(\theta,\phi)}(\sigma) \tag{B.1}$$

with the spin eigenstates

$$\Sigma_{(\theta,\phi)}(+) = \begin{pmatrix} \cos\frac{\theta}{2} e^{-\mathrm{i}\phi/2} \\ \sin\frac{\theta}{2} e^{\mathrm{i}\phi/2} \end{pmatrix}, \qquad \Sigma_{(\theta,\phi)}(-) = \begin{pmatrix} -\sin\frac{\theta}{2} e^{-\mathrm{i}\phi/2} \\ \cos\frac{\theta}{2} e^{\mathrm{i}\phi/2} \end{pmatrix},$$

defined with respect to the quantization axis

$$\hat{u} = \begin{pmatrix} \sin\theta\cos\phi \\ \sin\theta\sin\phi \\ \cos\theta \end{pmatrix}.$$

The effect of $\hat{\mathcal{P}}$ on the eigenstates (B.1) is to change an incoming state in the left lead (L) in one rocking situation into an outgoing state of the right lead (R) in the other rocking situation and *vice versa*. Furthermore the position of the spin on the Bloch sphere is changed from (θ,ϕ) into $(\theta,-\phi+\pi)$, and the amplitude of the state is complex conjugated.

On the other hand, the action of $\hat{\mathcal{P}}$ cannot change the scattering-matrix, since the

Hamiltonian is invariant under the action of $\hat{\mathcal{P}}$. Therefore the following relation holds true:

$$a_{\bar{n}\sigma}^{(\theta,-\phi+\pi)*}(E,\mp U_0) = \sum_{n'\in(\text{L}\cup\text{R})}\sum_{\sigma'=\pm1} S_{n\sigma,n'\sigma'}^{(\theta,\phi)}(E,\pm U_0)b_{\bar{n}'\sigma'}^{(\theta,-\phi+\pi)*}(E,\mp U_0) \quad \text{(B.2)}$$

Here, the mode index $\bar{n}$ is related to mode n of the opposite lead by means of the symmetry transformation. Comparing Eq. (B.2) with the inverse of Eq. (A.2),

$$a_{n\sigma}^{(\theta,-\phi+\pi)}(E,\mp U_0) = \sum_{n'\in(\text{L}\cup\text{R})}\sum_{\sigma'=\pm1} \left[S^{(\theta,-\phi+\pi)}\right]_{n\sigma,n'\sigma'}^{-1}(E,\mp U_0)b_{n'\sigma'}^{(\theta,-\phi+\pi)}(E,\mp U_0),$$

and using the unitarity of the scattering matrix, $\mathbf{S}^{-1} = \mathbf{S}^{\dagger} = (\mathbf{S}^*)^{\text{t}}$, we find the symmetry relation for the scattering amplitudes

$$S_{n\sigma,n'\sigma'}^{(\theta,-\phi+\pi)}(E,\mp U_0) = S_{\bar{n}'\sigma',\bar{n}\sigma}^{(\theta,\phi)}(E,\pm U_0). \quad \text{(B.3)}$$

Similar relations can be obtained for any other symmetry operator that commutes with the Hamiltonian $\hat{\mathcal{H}}$. For the other two operators used in this paper, $\hat{R}_x\hat{R}_U\sigma_z$ and $\hat{R}_x\hat{R}_y\hat{R}_U\sigma_z$, the above procedure can be applied accordingly. It yields

$$S_{n\sigma,n'\sigma'}^{(\theta,\phi+\pi)}(E,\mp U_0) = S_{\bar{n}\sigma,\bar{n}'\sigma'}^{(\theta,\phi)}(E,\pm U_0) \quad \text{(B.4)}$$

for $[\hat{\mathcal{H}},\hat{R}_x\hat{R}_U\sigma_z] = 0$ and

$$S_{n\sigma,n'\sigma'}^{(\theta,\phi+\pi)}(E,\mp U_0) = p_n p_{n'} S_{\bar{n}\sigma,\bar{n}'\sigma'}^{(\theta,\phi)}(E,\pm U_0) \quad \text{(B.5)}$$

for $[\hat{\mathcal{H}},\hat{R}_x\hat{R}_y\hat{R}_U\sigma_z] = 0$, where $p_n = (-1)^{n-1}$ is the parity of the eigenfunction $\chi_n(y)$ in Eq. (B.1).

References

[1] S. Datta and B. Das, Appl. Phys. Lett. **56**, 665 (1990).
[2] E. I. Rashba, Sov. Phys. Solid State **2**, 1109 (1960).
[3] G. Schmidt, D. Ferrand, L. W. Molenkamp, A. T. Filip, and B. J. van Wess, Phys. Rev. B **62**, R4790 (2000).
[4] R. Fiederling, M. Keim, G. Reuscher, W. Ossau, G. Schmidt, A. Waag, and L. W. Molenkamp, Nature **402**, 787 (1999).
[5] Y. Ohno, D. K. Young, B. Beschoten, F. Matsukura, H. Ohno, and D. D. Awschalom, Nature **402**, 790 (1999).
[6] S. D. Ganichev, S. N. Danilov, J. Eroms, W. Wegscheider, D. Weiss, W. Prettl, and E. L. Ivchenko, Phys. Rev. Lett. **86**, 4358 (2001).
[7] E.R. Mucciolo, C. Chamon, and C. M. Marcus, Phys. Rev. Lett. **89**, 146802 (2002).
[8] M. Governale, F. Taddei, and R. Fazio, Phys. Rev. B **68**, 155324 (2003).
[9] M. Scheid, A. Pfund, D. Bercioux, and K. Richter, `arXiv:cond-mat/0601118`.
[10] M. Scheid, M. Wimmer, D. Bercioux, and K. Richter, phys. stat. sol. (c) **3**, 4235 (2006).
[11] P. W. Brouwer, Phys. Rev. B **58**, R10135 (1998).
[12] S. K. Watson, R. M. Potok, C. M. Marcus, and V. Umansky, Phys. Rev. Lett. **91**, 258301 (2003).
[13] P. Reimann, Phys. Rev. **361**, 57 (2002).
[14] P. Reimann, M. Grifoni, and P. Hänggi, Phys. Rev. Lett. 79, **10** (1997).
[15] H. Linke, T. E. Humphrey, A. Löfgren, A. O. Sushkov, R. Newbury, R. P. Taylor, and P. Omling, Science **268**, 2314 (1999).
[16] B. Braunecker, D. E. Feldman, and F. Li, `arXiv:0706.2761`.

[17] A. Matulis, F. M. Peeters, and P. Vasilopoulos, Phys. Rev. Lett. **72**, 1518 (1994).

[18] P. D. Ye, D. Weiss, R. R. Gerhardts, M. Seeger, K. von Klitzing, K. Eberl, and H. Nickel, Phys. Rev. Lett. **74**, 3013 (1995).

[19] V. Kubrak, F. Rahman, B. L. Gallagher, P. C. Main, M. Henini, C. H. Marrows, and M. A. Howson, Appl. Phys. Lett. **74**, 2507 (1999).

[20] V. Kubrak, A. C. Neumann, B. L. Gallagher, P. C. Main, M. Henini, C. H. Marrows, and M. A. Howson, Physica E **6**, 755 (2000).

[21] J. D. Jackson: *Classical Electrodynamics* (John Wiley & Sons, Inc., 1999).

[22] F. Zhai and H. Q. Xu, Appl. Phys. Lett. **88**, 032502 (2006).

[23] M. Lu, L. Zhang, Y. Jin, and X. Yan, Eur. Phys. J. B **27**, 565 (2002).

[24] A. Slobodskyy, C. Gould, T. Slobodskyy, C. R. Becker, G. Schmidt, and L. W. Molenkamp, Phys. Rev. Lett. **90**, 246601 (2003).

[25] J. K. Furdyna, J. Appl. Phys. **64**, R29 (1988).

[26] O. Madelung: *Semiconductors: Data Handbook* (Springer-Verlag, 2003).

[27] E. I. Rashba, J. Supercond. **18**, 137 (2005).

[28] J. Schliemann, Int. J. Mod. Phys. B **20**, 1015 (2006).

[29] H. Xu, Phys. Rev. B **47**, 15630 (1993).

[30] A. Lassl, P. Schlagheck, and K. Richter, Phys. Rev. B **75**, 045346 (2007).

[31] V. A. Sablikov, V. I. Borisov, and A. I. Chmil', JETP Lett. **81**, 75 (2005).

[32] M. Governale and D. Boese, Appl. Phys. Lett. **77**, 3215 (2000).

[33] M. Büttiker, Y. Imry, R. Landauer, and S. Pinhas, Phys. Rev. B **31**, 6207 (1985).

[34] A. A. Kiselev and K. W. Kim, Phys. Rev. B **71**, 153315 (2005).

[35] T. P. Pareek, Phys. Rev. Lett. **92**, 076601 (2004).

[36] B. K. Nikolic, L. P. Zârbo, and S. Souma, Phys. Rev. B **72**, 075361 (2005).

[37] T. P. Pareek, Phys. Rev. Lett. **92**, 076601 (2004).

[38] E. M. Hankiewicz, L. W. Molenkamp, T. Jungwirth, and J. Sinova, Phys. Rev. B **70**, 241301(R) (2004); W. Ren, Z. Qiao, J. Wang, Q. Sun, and H. Guo, Phys. Rev. Lett. **97**, 066603 (2006); J. H. Bardarson, I. Adagideli, and P. Jacquod, Phys. Rev. Lett. **98**, 196601 (2007).

[39] F. Zhai and H. Q. Xu, Phys. Rev. Lett. **94**, 246601 (2005).